Sensitivity of the Arctic sea ice cover to the summer surface scattering layer

Madison M. Smith[1], Bonnie Light[1], Amy R. Macfarlane[2], Don K. Perovich[3], Marika M. Holland[4], Matthew D. Shupe[5,6]

[1]Polar Science Center, Applied Physics Laboratory, University of Washington, Seattle, USA
[2]WSL Snow and Avalanche Research Centre SLF, Davos, Switzerland
[3]Thayer School of Engineering, Dartmouth College, Hanover, NH, USA
[4]National Center for Atmospheric Research, Boulder, Colorado, USA
[5]University of Colorado, Cooperative Institute for Research in Environmental Sciences, Boulder, CO, USA
[6]NOAA Physical Sciences Laboratory, Boulder, CO, USA

Key Points:

- Surface scattering layer (SSL) is a persistent feature of bare, melting sea ice that is central to the sea ice-albedo feedback
- Observations and modeling both show sea ice albedo sensitivity to surface scattering layer thickness
- Models represent the optical properties of the SSL layer as a function of ice thickness only, but these properties also vary with morphology

Corresponding author: Madison M. Smith, mmsmith@uw.edu

Abstract

The 'surface scattering layer' (SSL) is the highly-scattering, coarse-grained ice layer that forms on the surface of melting, drained sea ice during spring and summer. Ice of sufficient thickness with an SSL has an observed persistent broadband albedo of ∼0.65, resulting in a strong influence on the regional solar partitioning. Experiments during the MOSAiC expedition showed that the SSL re-forms in approximately one day following manual removal. Coincident spectral albedo measurements provide insight into the SSL evolution, where albedo increased on sunny days with higher solar insolation. Comparison with experiments in radiative transfer and global climate models show that the sea ice albedo is greatly impacted by the SSL thickness. The presence of SSL is a significant component of the ice-albedo feedback, with an albedo impact of the same order as melt ponds. Changes in SSL and implications for Arctic sea ice within a warming climate are uncertain.

1 Introduction

The sea ice-albedo feedback is a well-documented mechanism in the Arctic system. The role of open water and melt pond formation in lowering the albedo and leading to further sea ice melt has been a focus of recent research. However, a similarly important factor is the relatively high albedo of the bare sea ice even after snow has melted (D. K. Perovich et al., 2001) due to the formation of what is referred to as a "surface scattering layer" (SSL) during the summer melt season.

Early observations of the SSL described how the absorption of shortwave radiation by bare ice above freeboard results in transformation of the ice surface into a more granular, highly scattering layer (Untersteiner, 1961; Maykut & Untersteiner, 1971; Grenfell & Maykut, 1977). This makes up the characteristic feature of what is often referred to as bare or white ice in the sea ice environment, observed primarily during summer (D. K. Perovich et al., 1996). The SSL is generally observed during the melt season with a thickness between 0.01-0.1 m (Light et al., 2008) on top of the drained layer (DL) below. Although it is commonly observed, it is not well documented compared to other sea ice surface features.

The characteristics and formation of the SSL play strong roles in the optical properties of the ice cover and its thermodynamic evolution. The scattering of the SSL is 1-2 orders of magnitude higher than that of the interior layer (Light et al., 2008). The inherent optical properties result in a remarkably consistent bare ice albedo during Arctic summer (D. Perovich et al., 2002; Light et al., 2022 (in review)), with broadband albedo typically around 0.65 across ice types. The impact of the SSL optical properties can be captured in 1D process models (e.g., Grenfell, 1991; Malinka et al., 2016), and applied in global climate models. For example, Briegleb and Light (2007) proposed inherent optical properties based on observations for a sea ice radiative transfer model within the CICE sea ice model (E. Hunke et al., 2017), now widely used in global climate models (Keen et al., 2021). Arctic sea ice represented in the standalone CICE model has been shown to be fairly sensitive to the thickness of the SSL layer (Urrego-Blanco et al., 2016).

This manuscript aims to address the question: what is the role of the SSL in the sea ice-albedo feedback driving future ice changes? We approach this with both field and model experiments which indicate changes in sea ice optical properties and mass balance evolution in the absence of the SSL. While full loss of the SSL is unrealistic, the dramatic changes suggested by this sensitivity experiment raise questions about the possible implications of the uncertainty in the SSL on a thin, more seasonal ice cover.

2 Methods

2.1 Observations of SSL optical properties

A 'SSL removal' experiment was completed in July 2020 during the MOSAiC expedition in the Central Arctic (Nicolaus et al., 2022) on relatively level ice approximately 1.6 m thick. The experimental setup is shown in Figure 1. Two side-by-side 3-m x 3-m squares were identified: one of these was kept undisturbed (site "A"), while the other was shoveled to remove as much of the SSL as possible, exposing the DL below (site "B"). Both sites were characterized prior to shoveling, and monitored at regular intervals over subsequent days. Characterization included regular spectral albedo measurements and measurement of SSL thickness, though it should be noted that the thickness of the spatially heterogeneous SSL is particularly hard to measure. Measurements were made following typical methods for snow, where a ruler is inserted vertically into the surface. As the SSL is typically denser than snow, it can be assumed that this will underestimate the total thickness relevant to the differing optical properties. Characterization was constrained to one edge of the defined areas (Fig. 1), such that albedo measurements made from the opposite corners (i.e., A2-A3 and B2-B3) were largely undisturbed.

Spectral albedo measurements were made with an Analytical Spectral Devices (ASD) FieldSpec3 spectroradiometer (Light et al., 2022 (in review); Smith et al., 2021). The ASD measures radiant energy with a spectral range of 350-2500 nm, at 1 nm resolution. Albedos are calculated using the ratio of incident to reflected energy at each wavelength. The sensor is attached to the unit with a fiber optic cable, and was mounted on the end of a 1.5 m long carbon fiber arm in a gooseneck aimed at a spectralon plate held at approximately 1 m height (Grenfell & Perovich, 2008). In the context of this experiment, this means that the radiometer collects light from a relatively small area outside the defined 3x3 grid, as 80% of the observed signal is estimated to come from within 1.3 m of the observation point (grey shading in Fig. 1a). Spectral albedos from two corners of each site (2-3) were averaged together.

Incident and reflected surface broadband solar irradiances (285-3000 nm) were captured by an Atmospheric Surface Flux Station (ASFS50; Hukseflux SR30-D1 pyranometers mounted at approximately 2m height; Cox et al., 2021) located on bare, melting ice approximately 250 m from the experiment location. There was no notable precipitation over the 7-day period of this experiment.

2.2 Coupled climate model experiment

Sensitivity tests to explore the impact of the SSL were completed with CESM2.0 (Danabasoglu et al., 2020) using a constant pre-industrial forcing, over a global model domain with nominal horizontal resolution of 1°. Runs have fully coupled atmosphere, sea ice, and land models, and a simplified slab ocean model (SOM). The use of the SOM requires significantly less computational time, and allows the model to converge much faster, yet reproduces the climate of the fully coupled model with fidelity (Bitz et al., 2012). Spatially varying prescribed mixed layer depths with temperatures evolving based on surface heat fluxes determined by the coupled climate mode are used; thus, ice-albedo feedbacks are permitted (e.g., Smith et al., 2022).

The sea ice model used was CICE 5.1.2 (E. C. Hunke et al., 2015). Sea ice simulated over the historical period has reasonable mean state and variability in both hemispheres (DeRepentigny et al., 2020); here we used tuned albedos for snow on sea ice which give a more realistic simulation of ice thickness (Kay et al., in review). Sea ice optics are treated using the delta-Eddington radiation scheme, which defines observationally-based inherent optical properties (IOPs) for the three ice layers - SSL, DL, and interior layer (IL) (Briegleb & Light, 2007; Holland et al., 2012). The model uses eight vertical layers, where the SSL is assumed as a 5 cm surface layer for ice greater than 1.5 m thick,

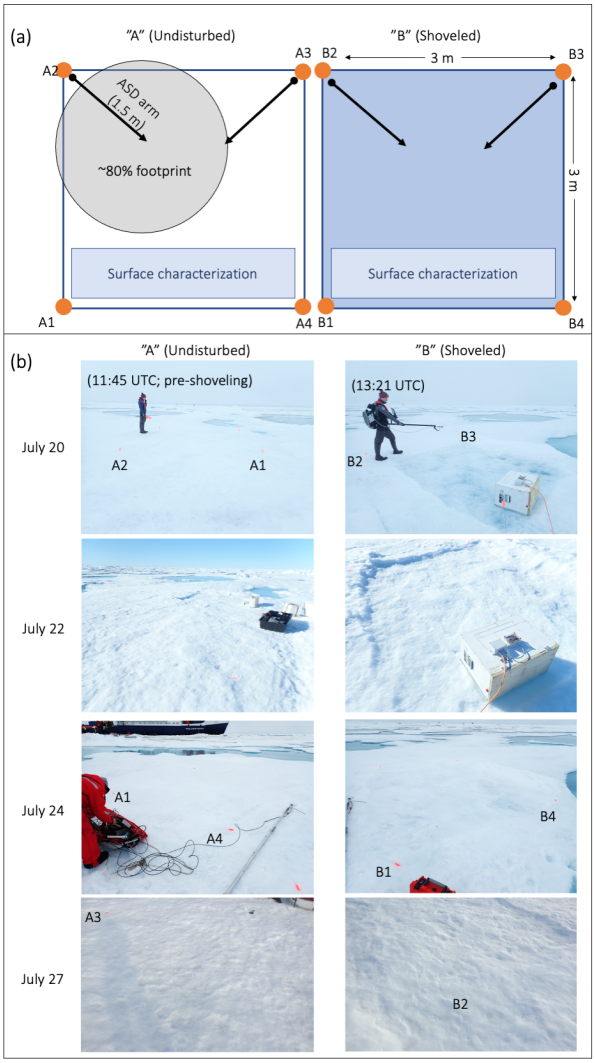

Figure 1. (a) Schematic of experimental set-up. (b) Photos of surface evolution at undisturbed site (left) and shoveled site (right) on July 20, 22, 24, and 27.

and 1/30 of the thickness for thinner ice. For practical reasons, the SSL is modeled as a persistent layer at the ice surface when snow is absent, although observations suggest more subtlety in types of surface layers throughout the melt season.

Two runs are used: a control with default settings as described here, and another where removal of the SSL is simulated ('no SSL') by defining the IOPs of the SSL as equivalent to those of the adjacent DL. This only considers the optical effects of the SSL, though removal could additionally have thermodynamic implications. The model also defines the optical properties of a scattering layer beneath ponds, but this layer was not altered in this experiment. Each run was 50 years long, and monthly averages over the last 25 years are used to examine changes in mean state of the sea ice.

2.3 1D radiative transfer model

A 1D four-stream discrete ordinates radiative transfer model (Grenfell, 1991) was used to simulate sea ice albedo with a range of SSL thicknesses. This provides a bridge between the field observations and coupled climate model simulations, as this 1D model produces comparable results to the delta-Eddington scheme in CESM2. The same configuration as in Light et al. (2008, 2015) is largely used here. The model explicitly calculates the effects of multiple scattering, such that IOPs of the vertical ice column are used as inputs. In general, we use values as defined in Tables 11 and 12 of Briegleb and Light (2007), which defined observationally-based extinction and scattering coefficients for the three sea ice layers averaged over 3 wavelength bands. The bulk refractive index of the low-density SSL is set to 1.0, while DL and IL are set to the pure ice value of 1.3. The asymmetry parameter, g, is the cosine weighted average of the phase function, and was assumed to be 0.94 at all wavelengths for computational efficiency with appropriate changes to scattering coefficients to compensate (Light et al., 2008).

1D model runs were used to simulate the albedo of sea ice with SSL between 0 and 10 cm with 0.5 cm resolution from 0-5 cm, and 1 cm resolution from 5-10 cm. A total sea ice thickness of 1.6 m is used. We assume 8 vertical layers, for best comparison with the approach used in the CESM2 model. The combined thickness of SSL and DL is 20 cm (the top vertical layer), such that the SSL ranges from 0-10 cm and the DL ranges from 10-20 cm.

3 Results

3.1 Observational experiment

The SSL removal experiment demonstrated the impact of the SSL on the sea ice surface. Photos in Figure 1b show indication of the SSL removal, where the sea ice surface appears notably bluer (darker) following shoveling. With the re-formation of the SSL, the surface regains the characteristic bright white appearance.

At the beginning of the experiment (July 20), SSL thickness at both sites was measured as 4 cm. On July 21, average SSL thickness was measured as 4 cm at site A and 2 cm at site B. Similarly, average SSL thickness on July 23 was measured as 4.5 cm at site A and 2.5 cm at site B. The thicknesses were approximately equal by the final date of the experiment, July 27. Note that thicknesses should be taken as approximations due to challenges of measuring this layer.

Figure 2 shows spectral albedo evolution over the undisturbed and shoveled areas. The spectral albedos were nearly identical prior to shoveling early on the 20th, with the albedos at site B being only slightly lower (0.02 at 950 nm). Manual removal of SSL results in a significant decrease in albedo: albedo decreased $\sim$0.08 at 550 nm, and $\sim$0.13 at 850 nm. The albedo at 850 nm is sensitive to roughly the depth of the SSL, as the penetration depth is less than at visible wavelengths.

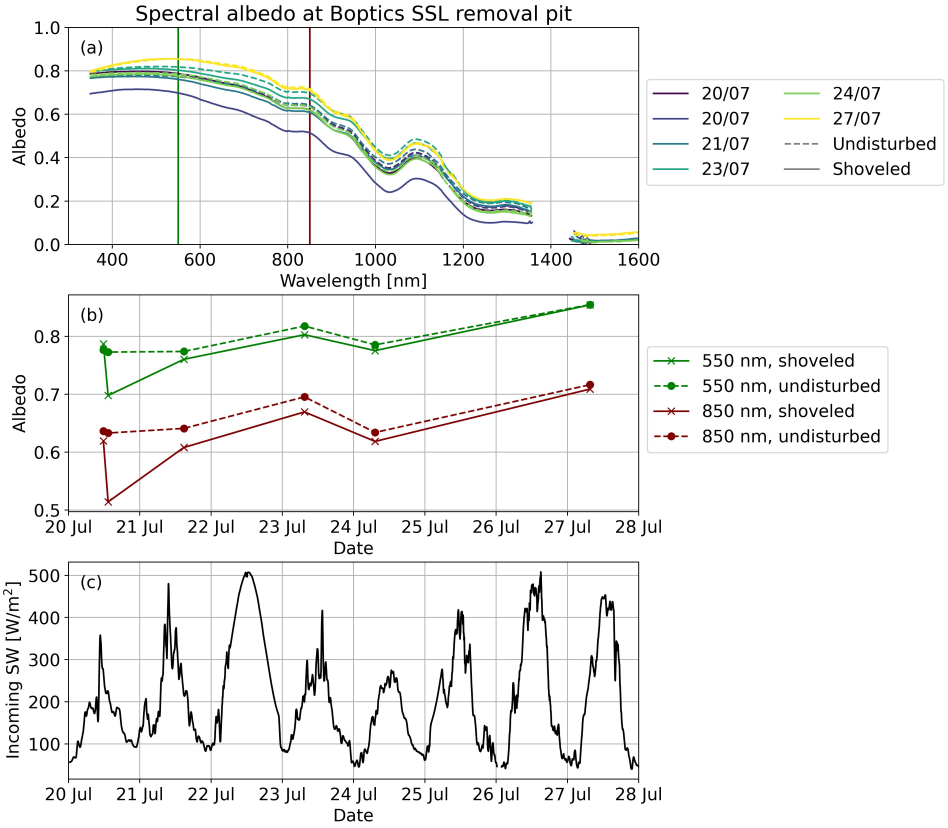

Figure 2. (a) Spectral albedo at undisturbed site (dashed) and shoveled site (solid) during SSL removal experiment from July 20-27, and (b) temporal evolution at selected wavelengths: 550 nm (green) and 850 nm (red). (c) Time series of incoming SW radiation from ASFS50 over the experiment.

Just one day later (July 21), the spectral albedos at site B had significantly increased to nearly previous levels: values at 550 and 850 nm were only 0.01 and 0.03 lower, respectively (Fig. 2b). This gap continued to close over subsequent days, to below 0.01 difference for all wavelengths by July 27 (7 days after initial shoveling). SSL formation is likely more rapid initially as more solar radiation can reach the drained layer. As the SSL thickens, the rate of thickening also likely slows as high scattering in the SSL provides protection to the ice below.

Notably, the day-to-day variability in spectral albedo at both sites over subsequent dates is greater than the difference between the two sites. The albedo increases about 0.05 from July 21 to 23 at 850 nm. The albedo at 850 nm decreases at both sites by about 0.06 from July 23 to 24, then increases again by about 0.08-0.09 over the next 3 days. These fluctuations appear to be tied to the variation in incoming shortwave (SW) radiation (Fig. 2c), where the highest spectral albedos likely follow when SW radiation is the highest (i.e., optically thinnest clouds). This is likely a result of two factors. The first is that higher solar radiation may thicken the SSL or change the crystal morphology in a manner that increases reflectively. The second is that the spectral albedo at high latitudes is inherently lower under the diffuse light of cloudier conditions, resulting in a lower effective solar zenith angle. Radiative transfer calculations indicate that clear sky with solar zenith angle of 67° (as was typical during this experiment) enhanced the albedo compared to fully diffuse, cloudy conditions over 200-700 nm by around 10%. Changes in albedo greater than 10% is likely to be indicative of morphological changes. The diffuse fraction of the incoming radiation has an instantaneous effect, while the morphological changes are likely to be delayed by hours. In particular, peaks in incident irradiance on July 22 and 26 are followed by days with relatively high albedos, and cloudy conditions on July 23 can similarly be linked to decreased albedos.

3.2 Model experiment

Figure 3 shows the mean annual cycle of Northern Hemisphere sea ice area and sea ice volume for the model experiment where the optical influence of SSL was removed. The simulated ice area and volume are substantially reduced throughout the annual cycle by removing the SSL. The reductions are most substantial at the sea ice minimum in September, where the average sea ice area decreases by around 30% and the sea ice volume decreases by around 50%. Although the focus of this study is on Arctic sea ice, it is worth noting that the changes in the Antarctic sea ice mean state are comparatively small due to the more significant snow pack and minor role of surface melt in the mass budget (Li et al., 2021).

The substantial reduction in Arctic sea ice volume and thickness is a result of increased sea ice surface melt (Fig. 3c). The increase in surface melt is largely a direct result of the reduction in albedo with removal of the SSL. Annually, surface melt increases by 16%, while basal and lateral melt are reduced by comparatively small amounts (-0.2% and -5%, respectively) primarily due to reductions in sea ice area. However, the annual total obscures the fact that the basal melt substantially increases over the melt season (May-September), while it decreases in winter due to reduction in ice area (Fig. 3c). Analysis suggests that the summer increase in basal melt is a result of increases in heat available in the ocean mixed layer, due to both the well-known ice-albedo feedback with decreases in ice area, and increases in transmission to the ocean through bare ice (not shown). Changes in other mass balance terms during the melt season are negligible, and changes in mass balance terms during the winter are a result of changes in sea ice area. Complementary analysis of the model surface energy budget shows that net shortwave radiation increases over the sunlit season, with no notable changes to other terms. This suggests that the excess of solar energy due to decreased albedo warms and melts the ice, rather than being mitigated by other energy budget terms.

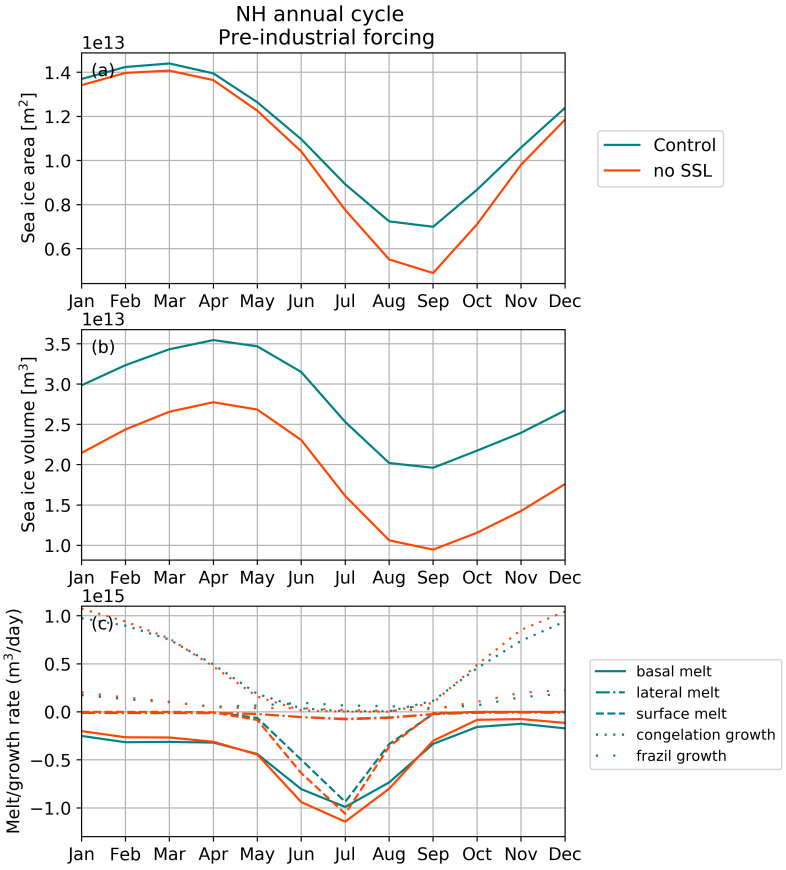

Figure 3. Seasonal cycle of Arctic sea ice in coupled model experiment. (a) Sea ice area, (b) sea ice volume, and (c) mass balance terms for the control run (green lines) and experimental run with no SSL (orange lines).

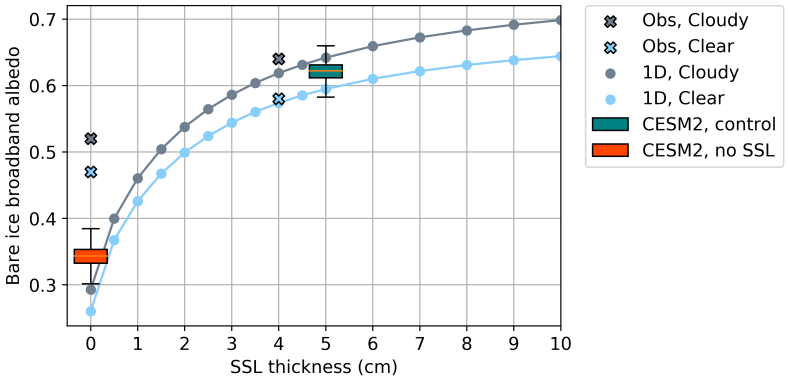

Figure 4. Broadband albedo of bare ice as a function of SSL thickness, suggested by model and observations. Spectral albedo from observations (Fig. 2) and 1D model results are converted to broadband by integrating over characteristic incident spectra for cloudy and clear conditions (Grenfell & Perovich, 1984). Black bars show intequartile range of CESM2 July bare ice albedo for 1.4-2.5 m thick ice across the Arctic basin.

The SSL removal in these experiments only directly impacts the albedo of the bare ice fraction of the sea ice cover. In July, this represents approximately 58% of the total simulated Arctic sea ice cover in both runs. Within this fraction, the July broadband albedo of the 1.4-2.5 m thick category of sea ice undergoes an average reduction of 0.25 (Fig. 4). We examine this category as it includes the thicknesses of ice observed in situ and modeled in 1D runs, and SSL is represented as a constant 5 cm for ice thicknesses beyond 1.4 m in the model.

3.3 Bare ice albedo dependence on SSL thickness

Figure 4 compares broadband albedos of bare ice as a function of SSL thickness from observations and models. As broadband albedos were not directly measured during the experiment, they are calculated from observed spectral albedos by integrating the product of the albedo and characteristic incident spectra over the relevant wavelengths. Characteristic incident spectral irradiances for clear and cloudy Arctic conditions are obtained from Grenfell and Perovich (2008) (Central Arctic, 2005). The same method is applied to the albedo for spectral bands output by the 1D radiative transfer model. Broadband albedos are simulated to be higher under cloudy conditions largely because of the attenuation of near-infrared wavelengths by clouds, weighting the integrated spectrum towards wavelengths with higher albedos (Grenfell & Perovich, 2008; Stapf et al., 2020)

The observations and model suggest similar dependence of bare ice albedo on SSL thickness: the albedo rapidly decreases with a thinning SSL (Fig. 4). The minimum albedo suggested by the 1D model is below 0.3 with no SSL present, but this value will be very sensitive to the optical properties of the DL, which are not precisely constrained (Light et al., 2008). Observations are placed on the figure at the estimated SSL thicknesses of 4 and 0 cm, respectively. The higher albedo relative to the model in the 'no SSL' case is likely a result of a combination of some remaining SSL after shoveling (<0.5 cm), the influence of surface outside the shoveled area (Fig. 1), and the slightly thicker ice (1.6 m). The albedo continues to increase past the 5 cm maximum modeled in CESM2; at 10 cm the albedo under cloudy conditions is 0.7, or approximately 0.06 higher than at 5 cm.

4 Discussion

While basin-wide loss of the SSL is unlikely, the drastic reduction in ice associated with SSL removal underscores its importance in maintaining sea ice. The role of the SSL in the Arctic sea ice-albedo feedback is of comparable magnitude to that of melt ponds, which have been the focus of substantial research. Specifically, in our model experiment, the complete removal of SSL from bare ice results in approximately the same reduction in July Arctic sea ice-averaged albedo as does the presence of melt ponds. The 16% average melt pond coverage results in a 0.12 lower sea ice albedo than that averaged across areas without melt ponds. Similarly, reducing the average bare ice albedo from 0.55 to 0.31 in our 'no SSL' run lowers the sea ice albedo by 0.14 as a cumulative result of changes in surface features. Note that this calculation does not reflect the actual simulated reduction in Arctic average surface albedo as it excludes the impact of feedbacks (e.g., thinning of ice and loss of sea ice area), which result in a less dramatic overall reduction in summer sea ice albedo in our experiment (0.02).

The rapid decline in albedo as SSL thins (Fig. 4) raises the question: what happens to the SSL as we move to a warmer climate with thinner, more seasonal sea ice? CESM2 models a thinner SSL on thinner sea ice using a linear relationship primarily for computational purposes, but the mechanism by which thinner ice should have a thinner SSL is not known. Additionally, it is unknown if salt content plays a role in SSL formation, such that changes would be expected in an Arctic with more high salinity seasonal ice. Anecdotal observations have suggested that the SSL formation is suppressed in the presence of sediment, but more quantitative observations are needed to understand the role of particulate inclusions in SSL evolution. The drivers of SSL spatial and temporal variability remains an open question, with insufficient data to capture possible feedbacks in models such as CESM2.

It appears that changes in optical depth of the SSL control much of the day-to-day variability of the sea ice albedo, which is not captured in models. The optical depth of the SSL is a combined result of the scattering properties and the physical thickness. The scattering properties are likely to vary as a result of changing crystal morphology, yet have not been well described. This will be explored in future work with MOSAiC observations by Macfarlane et al. (2021 (dataset in review)). The other primary factor is the physical thickness of the SSL. D. Perovich et al. (2002) suggested that the SSL thickens on sunny days and thins on cloudy days, and our data is indicative of this as well (Fig. 2). This relationship can be explained by a conceptual model for SSL thickness, where the observed thickness is proposed to be a result of the balance of surface melt (at the atmosphere-SSL interface) and SSL deepening (at the SSL-DL interface). At some given incident shortwave flux, there will be some equilibrium SSL thickness where surface melt and SSL deepening are in balance. The SSL depth is likely self-limiting by light extinction in the layer. If the surface melt were to increase relative to SSL deepening, such as from higher relative turbulent and longwave fluxes on cloudy days, the SSL could be expected to shoal or thin. If the SSL deepening were to increase relative to surface melt, such as from the higher shortwave flux on sunny days, the SSL could be expected to thicken. Untangling the relative role of changes in both SSL depth and structure as a function of incident solar radiation and the direct effect of cloud optical thickness (Stapf et al., 2020) is an important avenue for future research.

5 Conclusions

The SSL is a persistent feature of the summer sea ice cover that model results suggest is critical to maintaining the Arctic ice pack. The SSL is a key component of the sea ice-albedo feedback, by maintaining a relatively high albedo for bare ice, with similar order-of-magnitude impact as that of melt ponds. Experimental observations suggest that the SSL re-forms within a couple of days after removal, with an albedo that

is likely a result of a complex interplay between the layer thickness, crystal morphology, and cloud radiative effects. Nonetheless, the optical properties are relatively well defined such that models can generally capture the albedo of bare ice based on SSL and sea ice thickness. However, the spatial and temporal variability of SSL thickness is poorly characterized. This is especially important for thin ice, where the SSL thickness may dramatically impact the rate of ice melt.

Results motivate revisiting the parameterization of SSL thickness in models, where the dependence on ice thickness is variable, and currently largely dependent on model resolution. However, the sensitivity to SSL thickness opens the possibility for other facets to this feedback, where factors that lead to changes in SSL thickness may alter the feedback strength. More field observations and dedicated modeling improvements are needed to understand the primary factors determining the SSL thickness, and especially how it varies as a function of total ice thickness and atmospheric (cloud) conditions.

Acknowledgments

Data used in this manuscript were produced as part of the international Multidisciplinary drifting Observatory for the Study of the Arctic Climate (MOSAiC) with the tag MOSAiC20192020 and the Project_ID: AWI_PS122_00. We thank all people involved in the expedition of the Research Vessel Polarstern (Knust, 2017) during MOSAiC in 2019-2020 as listed in Nixdorf et al. (2021). The CESM project is supported primarily by the National Science Foundation. Computing and data storage resources, including the Cheyenne supercomputer (https:// doi.org/10.5065/ D6RX99HX), were provided by the Computational and Information Systems Laboratory (CISL) at NCAR. We thank all the scientists, software engineers, and administrators who contributed to the development of CESM2. We especially thank Dave Bailey for assistance with CESM2 runs.

MMS was supported by NSF OPP-1724467 and OPP-1724748. BL was supported by NSF OPP-1724467 and OPP-2138787. MMH was supported by NSF OPP-1724748. MDS was supported by the National Science Foundation (OPP-1724551), DOE Atmospheric System Research Program (DE-SC0021341) and the NOAA Physical Sciences Laboratory and Global Ocean Monitoring and Observing Program. ARM was supported by: Swiss Polar Institute (SPI reference DIRCR-2018-003), European Union's Horizon 2020 research and innovation program projects ARICE (grant 730965) for berth fees associated with the participation of the DEARice project, and WSL Institute for Snow and Avalanche Research SLF (WSL_201812N1678). DKP was supported by NSF OPP-1724540 and 1724424.

Data availability statement

All relevant observational datasets have been archived at the National Science Foundation's Arctic Data Center. Spectral albedo data and ancillary measurements including depths and photos from the SSL removal experiment (shortname: BOP) are archived at doi.org/10.18739/A2FT8DK8Z and doi.org/10.18739/A2B27PS3N (Smith et al., 2021). Atmospheric Surface Flux Station 50 data is available from the Arctic Data Center as Cox et al. (2021).

References

Bitz, C. M., Shell, K., Gent, P., Bailey, D., Danabasoglu, G., Armour, K., ... Kiehl, J. (2012). Climate sensitivity of the community climate system model, version 4. *Journal of Climate*, *25*(9), 3053–3070.

Briegleb, B. P., & Light, B. (2007). *A delta-eddington multiple scattering parameterization for solar radiation in the sea ice component of the community climate system model* (Tech. Rep. Nos. TN-472+STR). NCAR.

Cox, C., Gallagher, M., Shupe, M., Persson, O., Solomon, A., Ayers, T., ... Uttal, J. (2021). *Atmospheric surface flux station 50 measurements (level 1 raw), multidisciplinary drifting observatory for the study of arctic climate (mosaic), central arctic, october 2019 - september 2020* (Tech. Rep.). doi:10.18739/A2445HD46: Arctic Data Center.

Danabasoglu, G., Lamarque, J.-F., Bacmeister, J., Bailey, D., DuVivier, A., Edwards, J., ... others (2020). The community earth system model version 2 (cesm2). *Journal of Advances in Modeling Earth Systems*, *12*(2), e2019MS001916.

DeRepentigny, P., Jahn, A., Holland, M. M., & Smith, A. (2020). Arctic sea ice in two configurations of the cesm2 during the 20th and 21st centuries. *Journal of Geophysical Research: Oceans*, *125*(9), e2020JC016133.

Grenfell, T. C. (1991). A radiative transfer model for sea ice with vertical structure variations. *Journal of Geophysical Research: Oceans*, *96*(C9), 16991–17001.

Grenfell, T. C., & Maykut, G. A. (1977). The optical properties of ice and snow in the arctic basin. *Journal of Glaciology*, *18*(80), 445–463.

Grenfell, T. C., & Perovich, D. K. (1984). Spectral albedos of sea ice and incident solar irradiance in the southern beaufort sea. *Journal of Geophysical Research: Oceans*, *89*(C3), 3573–3580.

Grenfell, T. C., & Perovich, D. K. (2008). Incident spectral irradiance in the arctic basin during the summer and fall. *Journal of Geophysical Research: Atmospheres*, *113*(D12).

Holland, M. M., Bailey, D. A., Briegleb, B. P., Light, B., & Hunke, E. (2012). Improved sea ice shortwave radiation physics in ccsm4: The impact of melt ponds and aerosols on arctic sea ice. *Journal of Climate*, *25*(5), 1413–1430.

Hunke, E., Lipscomb, W., Jones, P., Turner, A., Jeffery, N., & Elliott, S. (2017). *Cice, the los alamos sea ice model* (Tech. Rep.). Los Alamos National Lab.(LANL), Los Alamos, NM (United States).

Hunke, E. C., Lipscomb, W. H., Turner, A. K., Jeffery, N., & Elliott, S. (2015). *CICE: the Los Alamos Sea Ice Model Documentation and Software User's Manual Version 5.1 LA-CC-06-012* (Tech. Rep.). Los Alamos National Laboratory. Retrieved from `http://oceans11.lanl.gov/trac/CICE`

Kay, J. E., DeRepentigny, P., Holland, M., Bailey, D., DuVivier, A., Blanchard-Wrigglesworth, E., ... Webster, M. (in review). Less surface sea ice melt in the cesm2 improves arctic sea ice simulation with minimal non-polar climate impacts. *Journal of Advances in Modeling Earth Systems*, doi.org/10.1002/essoar.10507477.1.

Keen, A., Blockley, E., Bailey, D., Boldingh Debernard, J., Bushuk, M., Delhaye, S., ... others (2021). An inter-comparison of the mass budget of the arctic sea ice in cmip6 models. *The Cryosphere*, *15*(2), 951-982.

Knust, R. (2017). Polar research and supply vessel polarstern operated by the alfred-wegener-institute. *Journal of large-scale research facilities*, *3*, https://doi.org/10.17815/jlsrf-3-163.

Li, S., Huang, G., Li, X., Liu, J., & Fan, G. (2021). An assessment of the antarctic sea ice mass budget simulation in cmip6 historical experiment. *Frontiers in Earth Science*, *9*, 249.

Light, B., Grenfell, T. C., & Perovich, D. K. (2008). Transmission and absorption of solar radiation by arctic sea ice during the melt season. *Journal of Geophysical Research: Oceans*, *113*(C3).

Light, B., Perovich, D. K., Webster, M. A., Polashenski, C., & Dadic, R. (2015). Optical properties of melting first-year a rctic sea ice. *Journal of Geophysical Research: Oceans*, *120*(11), 7657–7675.

Light, B., Smith, M., Perovich, D., Webster, M., Holland, M., Linhardt, F., ... Bailey, D. (2022 (in review)). Arctic sea ice albedo: spectral composition, spatial heterogeneity, and temporal evolution observed during the mosaic drift.

Elementa Science of the Anthropocene.

Macfarlane, A. R., Tavri, A., Polashenski, C., Krampe, D., Seawell, D. C., Wagner, D. N., ... Schneebeli, M. (2021 (dataset in review)). *Snowpit raw data during the mosaic expedition* (Tech. Rep.). https://doi.pangaea.de/10.1594/PANGAEA.935934: PANGAEA.

Malinka, A., Zege, E., Heygster, G., & Istomina, L. (2016). Reflective properties of white sea ice and snow. *The Cryosphere*, *10*(6), 2541–2557.

Maykut, G. A., & Untersteiner, N. (1971). Some results from a time-dependent thermodynamic model of sea ice. *Journal of Geophysical Research*, *76*(6), 1550–1575.

Nicolaus, M., Perovich, D. K., Spreen, G., Granskog, M. A., von Albedyll, L., Angelopoulos, M., ... Wendisch, M. (2022). Overview of the mosaic expedition - snow and sea ice. *Elementa Science of the Anthropocene*, https://doi.org/10.1525/elementa.2021.000046.

Perovich, D., Grenfell, T., Light, B., & Hobbs, P. (2002). Seasonal evolution of the albedo of multiyear arctic sea ice. *Journal of Geophysical Research: Oceans*, *107*(C10), SHE–20.

Perovich, D. K., et al. (1996). The optical properties of sea ice.

Perovich, D. K., Richter-Menge, J. A., & Tucker, W. B. (2001). Seasonal changes in arctic sea-ice morphology. *Annals of Glaciology*, *33*, 171–176.

Smith, M., Holland, M., & Light, B. (2022). Arctic sea ice sensitivity to lateral melting representation in a coupled climate model. *The Cryosphere Discussions*, 1–21.

Smith, M., Light, B., Perovich, D., Webster, M., Anhaus, P., Clemens-Sewall, D., ... Tavri, A. (2021). *Spectral albedo measurements of the sea ice surface during the multidisciplinary drifting observatory for the study of arctic climate (mosaic) campaign in the central arctic ocean, april – september 2020* (Tech. Rep.). doi:10.18739/A2FT8DK8Z: Arctic Data Center.

Stapf, J., Ehrlich, A., Jäkel, E., Lüpkes, C., & Wendisch, M. (2020). Reassessment of shortwave surface cloud radiative forcing in the arctic: consideration of surface-albedo–cloud interactions. *Atmospheric Chemistry and Physics*, *20*(16), 9895–9914.

Untersteiner, N. (1961). On the mass and heat budget of arctic sea ice. *Archiv für Meteorologie, Geophysik und Bioklimatologie, Serie A*, *12*(2), 151–182.

Urrego-Blanco, J. R., Urban, N. M., Hunke, E. C., Turner, A. K., & Jeffery, N. (2016). Uncertainty quantification and global sensitivity analysis of the los alamos sea ice model. *Journal of Geophysical Research: Oceans*, *121*(4), 2709–2732.